PNAS RESEARCH ARTICLE | CHEMISTRY BIOCHEMISTRY

The mechanism of allosteric regulation of calcium-independent phospholipase A_2 by ATP and calmodulin binding to the ankyrin domain

Varnavas D. Mouchlis[a,b,1], Yuan-Hao Hsu[a,b], Daiki Hayashi[a,b,c], Jian Cao[a,b], Sheng Li[d], J. Andrew McCammon[a,b,1], and Edward A. Dennis[a,b,1]

Affiliations are included on p. 7.

Contributed by J. Andrew McCammon; received June 27, 2024; accepted October 7, 2024; reviewed by Xiaolin Cheng and Chung Wong

Group VIA calcium-independent phospholipase A_2 (iPLA$_2$) is a member of the PLA$_2$ superfamily that exhibits calcium-independent activity in contrast to the other two major types, secreted phospholipase A_2 (sPLA$_2$) and cytosolic phospholipase A_2 (cPLA$_2$), which both require calcium for their enzymatic activity. Adenosine triphosphate (ATP) has been reported to allosterically activate iPLA$_2$, and this has now been verified with a lipidomics-based mixed-micelle assay, but its mechanism of action has been unknown. Hydrogen/deuterium exchange mass spectrometry (HDX-MS) was employed to identify ATP interaction peptide regions located within the ankyrin repeat domain at which ATP interacts. Molecular dynamics simulations revealed the mechanism by which ATP binds to its site and the main residues that interact. Site-directed mutagenesis was used to verify the importance of these residues in the role of ATP in regulating iPLA$_2$ activity. Importantly, calcium was found to abolish the enhancing regulatory function of ATP and to promote the inhibitory activity by calmodulin. Given previous evidence that calcium does not bind directly to iPLA$_2$, its effect appears to be indirect via association with ATP and/or calmodulin. Using HDX-MS, we found that calmodulin interacts with the N terminus peptide region of iPLA$_2$ consisting of residues 20 to 28. These two regulatory iPLA$_2$ sites open the road to the development of potential targets for therapeutic intervention.

phospholipases | molecular dynamics | HDX-MS | lipidomics | drug discovery

Significance

The iPLA$_2$ is a member of the PLA$_2$ superfamily that exhibits calcium-independent activity in contrast to the other two major types, sPLA$_2$, which requires calcium for catalysis and cPLA$_2$, which requires calcium to activate its C2 domain. A lipidomics-based mixed-micelle assay shows that iPLA$_2$ is activated by ATP, HDX-MS identified ATP interaction peptide regions within the ankyrin repeat domain, molecular dynamics simulations revealed the main residues that interact, and site-directed mutagenesis was used to verify the predictions. Importantly, calcium abolishes the enhancing regulatory function of ATP and promotes inhibitory activity by calmodulin when binding to the N-terminal ankyrin repeat region residues 20 to 28. The ankyrin repeat is an important regulatory domain.

The Group VIA calcium-independent phospholipase A_2 (GVIA iPLA$_2$, also known as iPLA$_2$β, PLA$_2$G6A, or PNPLA9) is a well-characterized membrane-associated enzyme that hydrolyzes membrane phospholipids (1, 2). Extensive substrate specificity studies using lipidomics assays, hydrogen–deuterium exchange mass spectrometry (HDX-MS), and molecular dynamics (MD) simulations revealed that iPLA$_2$ exhibits preference for linoleic (18:2) and myristic (14:0) acid at the *sn*-2 position of a phospholipid molecule (3–7). iPLA$_2$ is involved in various diseases including "phospholipase A_2-associated neurodegeneration" diseases (8), especially neurodegeneration with brain iron accumulation (NBIA) disorders (9), infantile neuroaxonal dystrophy (10), Barth syndrome (11, 12), and Parkinson's disease, as well as diabetes (13, 14), and thus, this enzyme is an attractive pharmaceutical target (15, 16). Fluoroketones are highly potent and selective inhibitors of iPLA$_2$ and have been extensively used as tool compounds to understand the implication of the enzyme in diabetes (14), and multiple sclerosis (17). HDX-MS and MD simulations were utilized to understand the binding and interactions of fluoroketone inhibitors with the active site of iPLA$_2$ (18). Extensive computer-aided design led to the development of enzyme-inhibitor models that we used to improve the potency and selectivity of fluoroketone inhibitors against iPLA$_2$ (19). Virtual screening coupled with lipidomics assays were successfully employed to identify additional chemotypes for iPLA$_2$ inhibition (20, 21).

GVIA iPLA$_2$ was originally cloned from rodent cells as a PLA$_2$ enzyme composed of 752 amino acids with eight ankyrin repeats at the N-terminal and its catalytic domain based on amino acid homology at the C-terminal (22). Later, it was reported that humans express two enzymatically active GVIA iPLA$_2$s by alternative splicing, one is a 752 amino acids protein homologous to rodent GVIA iPLA$_2$ (referred to as human GVIA-1) and another (human GVIA-2) possessing a 54 amino acids insertion disrupting the eighth ankyrin repeat resulting in a longer 806 amino acid protein, but with one fewer intact ankyrin repeat (23). Recently, the crystal structure of rodent GVIA iPLA$_2$ was solved and revealed that the N-terminal region possesses an additional ankyrin repeat which has a less conserved sequence (16). Therefore, the short rodent form of GVIA iPLA$_2$ is now specified as GVIA-1 iPLA$_2$ (also referred to as the "short isoform") with nine ankyrin repeats and the long human form of GVIA iPLA$_2$ is specified as GVIA-2 iPLA$_2$ (also referred to as the "long isoform") with

Author contributions: V.D.M., Y.-H.H., D.H., J.C., S.L., J.A.M., and E.A.D. designed research; V.D.M., Y.-H.H., D.H., J.C., S.L., J.A.M., and E.A.D. performed research; V.D.M., D.H., J.C., S.L., J.A.M., and E.A.D. analyzed data; and V.D.M., Y.-H.H., D.H., J.C., S.L., J.A.M., and E.A.D. wrote the paper.

Reviewers: X.C., The Ohio State University; and C.W., University of Missouri–St. Louis.

The authors declare no competing interest.

[1]To whom correspondence may be addressed. Email: vmouchlis@gmail.com, jmccammon@ucsd.edu, or edennis@ucsd.edu.

This article contains supporting information online at https://www.pnas.org/lookup/suppl/doi:10.1073/pnas.2411539121/-/DCSupplemental.

Published November 19, 2024.

eight ankyrin repeats (8). The studies described herein were all carried out on the human GVIA-2 iPLA$_2$.

The association of iPLA$_2$ with the membrane is an important step in the mechanism of action of the enzyme. The association mechanism and the interactions of iPLA$_2$ with the membrane were elucidated through HDX-MS and MD simulations (24, 25). These studies were carried out on the human GVIA-2 iPLA$_2$, (now believed to contain eight ankyrin repeats and a ninth interrupted with a 54 amino acid insert based on the X-ray crystal structure of the rodent short form GVIA-1; see above) and revealed the association of the enzyme through an anchor region (residues 708 to 730) adjacent to the active site (24, 25). This peptide region forms an amphipathic helix within the membrane with its hydrophilic residues (Arg710 and Lys719) interacting with the headgroups of the fatty acids and its hydrophobic residues (Pro711, Pro714, Trp715, Leu717, Val721, and Phe722) interacting with the acyl-chains of the fatty acids (6). It is noteworthy that the homology model and later the crystal structure revealed an iPLA$_2$ ankyrin repeat domain (ARD) that did not show any interactions with the membrane (6, 16). iPLA$_2$ is localized in mitochondria and the endoplasmic reticulum, and its calcium-independent activity was reported to be regulated by ATP and inhibited by calmodulin (26–29). A combination of experimental and computational methods was employed to understand the regulation of iPLA$_2$ and to demonstrate the detailed ATP binding and activation mechanism, and the interplay between ATP activation and calcium inhibition as well as calmodulin binding. A mixed-micelle assay was used to study the kinetics and activation of iPLA$_2$ by ATP. HDX-MS and site-directed mutagenesis revealed that ATP activates iPLA$_2$ by binding to the ARD. The binding mode and interactions of ATP with the ankyrin repeat binding site were elucidated using MD simulations. Finally, calcium-activated calmodulin binds the N-terminal iPLA$_2$ to inhibit its activity and the ankyrin-1 protein competes with the ankyrin repeats for calmodulin binding, resulting in the lessening of its inhibition of iPLA$_2$.

Results

Allosteric Activation of iPLA$_2$ by ATP. ATP has been reported to bind and prevent the oxidation of critical residues on iPLA$_2$ (22, 29, 30). To test whether iPLA$_2$ activity is ATP dependent, we purified the human GVIA-2 iPLA$_2$ in the absence of ATP. To confirm the activation effect of ATP using a lipidomics-based liquid chromatographic-mass spectrometric (LC-MS) assay, we studied the concentration-dependent activation of ATP using mixed-micelle substrates containing PC 16:0/18:2 [1-palmitoyl-2-linoleoyl-sn-glycero-3-phosphatidylcholine (PLPC)], which was found to be the optimal substrate for iPLA$_2$, along with PC 16:0/20:4 [1-palmitoyl-2-arachidonoyl-sn-glycero-3-phosphocholine (PAPC)] (6). The results showed that 100 μM of ATP was sufficient to accomplish complete activation of iPLA$_2$ for both PLPC and PAPC substrates (Fig. 1 *A* and *B*). The calculated EC$_{50}$ values of the PLPC and PAPC substrates were 7.90 ± 0.9 μM and 7.88 ± 1.9 μM, respectively. The specific activity of iPLA$_2$ was also tested at various concentrations of ATP in a radioactive mixed-micelle assay containing PAPC (*SI Appendix*, Fig. S1*A*). These results further validated the ATP-dependent activation of iPLA$_2$. Using a one site-specific binding curve the Vmax was calculated to be 1.5 μmol/min/mg, and the

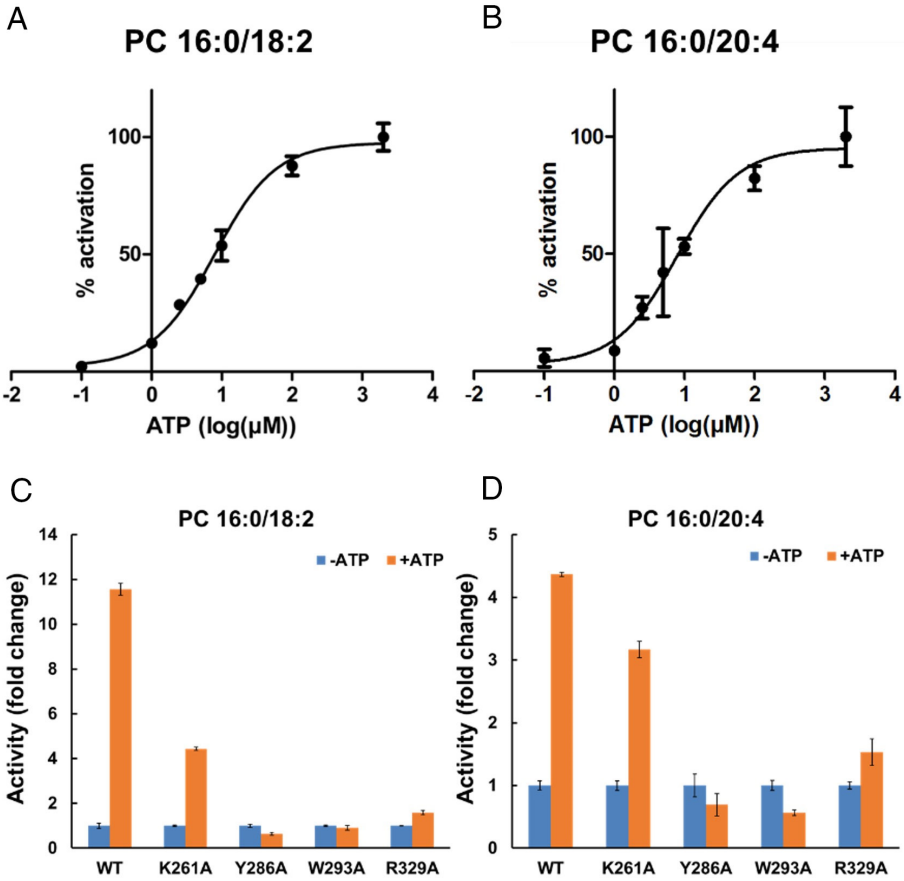

Fig. 1. The activation effect of ATP on iPLA$_2$ WT and mutants using the LC-MS assay. The concentration-dependent effect of ATP on the activity of iPLA$_2$ using mixed-micelle substrate containing (*A*) PLPC and (*B*) PAPC. The effect of 2 mM ATP on the activity of iPLA$_2$ WT and mutants using the mixed-micelle substrate containing (*C*) PLPC and (*D*) PAPC. Values are presented as fold change of each activity in the absence of ATP normalized by the amount of the enzyme detected in the western blot (*SI Appendix*, Fig. S6*A*). The values are shown as mean ± SD.

apparent Km was calculated to be 0.9 μM indicating that 100 μM ATP can fully activate $iPLA_2$.

Metal ions such as magnesium are necessary for ATP binding and catalysis of protein kinases and the crystal structure of PKA illustrates the coordination of ATP with two magnesium di-cations in the ATP binding pocket (31). Unlike protein kinases, ATP is not a substrate but an activator for $iPLA_2$ (Fig. 1 *A* and *B* and *SI Appendix*, Fig. S1*A*). The $iPLA_2$ activity was tested in the presence of ethylenediaminetetraacetic acid (EDTA) and it was confirmed that metal ions were not required for the enzymatic activity. In addition, the di-cation effects on $iPLA_2$ activity were examined, because di-cations could potentially coordinate with ATP and hence affect $iPLA_2$ catalysis. Magnesium inhibited $iPLA_2$ with an IC_{50} of 1.0 mM in the presence of 100 μM ATP (*SI Appendix*, Fig. S1*B*). Calcium also inhibited the $iPLA_2$ activity with an IC_{50} of 0.86 mM at an ATP concentration of 20 μM (*SI Appendix*, Fig. S1*C*). A fivefold increase of ATP to 100 μM doubled the IC_{50} to 1.6 mM. At a lower ATP concentration of 5 μM, the $iPLA_2$ activity was about 64% and half of it was inhibited in the presence of 100 μM of calcium. This result indicated that both magnesium and calcium di-cations could potentially inhibit $iPLA_2$ and the inhibition is reduced as the ATP concentration increases. A hypothesis that magnesium and calcium di-cations are likely to interact with the phosphate group of ATP preventing them from inhibiting $iPLA_2$ activity is possible. These results indicate that ATP is not only an allosteric activator but that the observed $iPLA_2$ activity also reflects potential magnesium and calcium di-cation inhibition. Various mutants were generated to assess the impact of ATP on $iPLA_2$ activity. Specifically, residues K261, Y286, W293, and R329 were substituted with alanine, and their activity was examined in the presence and absence of ATP using a lipidomics-based assay with PLPC or PAPC substrates. K261, Y286, and W293 were located within regions of decreased deuteration levels, while R329 was identified as an additional charged residue through MD simulations. All mutants exhibited significantly reduced responsiveness to ATP across both substrates. Notably, K261A still displayed ATP activation (Fig. 1 *C* and *D*).

Calmodulin Inhibition of $iPLA_2$. The activation of calmodulin is associated with the binding of four calcium di-cations that induces a conformational change (32). Activated calmodulin was found to interact with calmodulin-binding proteins to change their subcellular localization or enzymatic activity (32). Calmodulin-binding proteins that are not directly regulated by calcium, they usually respond to intracellular calcium through calmodulin. It has been reported that $iPLA_2$ binds to and is inhibited by calmodulin (27). Since calcium is a negative regulator of $iPLA_2$ activity calmodulin inhibition was tested in the presence of 500 μM ATP and 500 μM calcium, conditions under which $iPLA_2$ maintains its full activity. Under the same conditions, $iPLA_2$ activity was inhibited by calmodulin at an IC_{50} of 1.2 μM (*SI Appendix*, Fig. S2*A*). The reactivation of the calmodulin-inhibited $iPLA_2$ by ATP was tested and these results showed that the $iPLA_2$ activity was partially rescued by increasing the ATP concentration (*SI Appendix*, Fig. S2*B*). It is worth mentioning that at high ATP concentration (100 to 500 μM ATP) 60 to 70% of $iPLA_2$ activity was rescued indicating that the calmodulin binding effect was only partially reversed by the ATP binding. At lower ATP concentrations of 5 to 50 μM, only 30% of the $iPLA_2$ activity was rescued. The calcium inhibition of $iPLA_2$ in the presence of 100 μM ATP and 4 μM calmodulin was also examined (*SI Appendix*, Fig. S2*C*). At 10 μM of calcium, the activity of $iPLA_2$ was inhibited by 50%. These results indicated that the concentration of ATP, calcium, and calmodulin as well as the ratio between these three components are crucial for the regulation of $iPLA_2$ activity.

The splice variant ankyrin-1 protein is the catalytic domain deletion mutant of the $iPLA_2$. The ankyrin-1 protein does not have activity, but it has been proposed to be an inhibitor of $iPLA_2$ through the formation of hetero-oligomers (1). Since the ankyrin repeat motifs are known for participating in protein–protein interactions (33), the hypothesis of ankyrin-1 rescuing the $iPLA_2$ activity in the presence of calmodulin was examined. This hypothesis was made based on the assumption that calmodulin could potentially bind to the N-terminal region of ankyrin-1 according to HDX-MS data described below. The experimental data showed that ankyrin-1 rescued $iPLA_2$ activity by interacting with calmodulin preventing the direct interaction of calmodulin with the $iPLA_2$ ankyrin repeats. It is noteworthy that in the presence of 100 μM calcium and 100 μM ATP, $iPLA_2$ was inhibited 69% by 4 μM calmodulin and 52% by 2 μM calmodulin (*SI Appendix*, Fig. S2*D*). Addition of 0.6 μM ankyrin-1 protein activated the 4 μM calmodulin-inhibited $iPLA_2$ by 60% and the $iPLA_2$ activity recovered by 20%. At 2 μM calmodulin, 0.6 μM ankyrin-1 activated the inhibited $iPLA_2$ by 71% and the $iPLA_2$ activity recovered by 34%. These results indicated that ankyrin-1 is a positive regulator of $iPLA_2$ activity in the presence of calmodulin.

$iPLA_2$ Coverage Map of Pepsin Fragmentation and Deuterium On-Exchange. For the HDX-MS experiments, a recombinant purified wild-type (WT) $iPLA_2$ (Group IVA-2, the longer of two splice variants of human $iPLA_2$) was used that was confirmed to be active using the mixed-micelle assay. The procedure of protein digestion by pepsin was optimized as previously described (24). The pepsin digestion of $iPLA_2$ was optimized and 181 peptides were identified, including some multiple charged peptides. Among them, 110 peptides had sufficient signal to noise ratio for analysis, which covered 88% of the total protein sequence. From these 110 peptides, 46 different peptides with the least number of overlapped residues were selected to determine the deuteration level of $iPLA_2$ (*SI Appendix*, Fig. S3*A*). Overall, the representative 46 peptides selected account for 71% coverage of the $iPLA_2$.

Deuterium exchange experiments were carried out by incubation of 35 μL of $iPLA_2$ with 105 μL of 95% D_2O buffer for six time points from 10 s to 3,000 s at 23 °C. The sample was quenched and injected onto the HPLC online digestion system (34). Each time point represents an individual experiment and each experiment was performed in triplicates with three different batches of enzyme on different days. The exchange results in various regions were shown by the deuteration levels calculated by the ratio of incorporated deuterons to maximum deuteration in a particular peptide (*SI Appendix*, Fig. S4*A*). The deuteration level increased over time because the deuterons accumulated through the time course of the amide hydrogen–deuterium exchange. Due to the fast off-exchange rate of the two N-terminal residues on each of the peptides, those residues would not be able to retain any deuterons under the experimental conditions employed; hence, these residues were not shown in the results. Some peptides which showed a poor signal to noise ratio after deuteration were also excluded from the analysis.

The deuteration levels at six time points were translated to a heat map and shown on our previously constructed models (*SI Appendix*, Fig. S3*B*) (24). $iPLA_2$ contains an N-terminal region from residues 1 to 121 of unknown structure, followed by eight ankyrin repeats from 122 to 382, as well as a linker region from 383 to 474 and a catalytic domain from 475 to 806 containing the active site Ser519 (*SI Appendix*, Fig. S3*B*). The homology model of $iPLA_2$ contains residues 88 to 474 with 51% homology to the crystal structure of human Ankyrin-R (PDB entry:1N11) (33) and residues 475 to 806 with 40% homology to the crystal

structure of patatin, a potato lipase (PDB entry: 1OXW) (35). At the time of this study the crystal structure of $iPLA_2$ was not available and the homology models were used. The crystal structure of $iPLA_2$ later confirmed our homology models since they were found to be identical to the crystal structure (16). The fast-exchanging regions are the linker region and the membrane binding region, and the slow deuteration region is the core of the catalytic domain.

Identification of ATP Binding Site Using HDX-MS. Since ATP was found to be a positive regulator of the $iPLA_2$ activity, and since $iPLA_2$ was reported to exhibit high affinity for ATP affinity chromatography (22), HDX-MS was employed to identify the ATP binding site. On-exchange experiments were performed in the absence and presence of ATP to determine the ATP binding effects. The exchange results of the ATP-bound $iPLA_2$ are shown in *SI Appendix*, Fig. S4*B*. Two peptide regions of $iPLA_2$ showed significant changes at 3,000 s upon addition of ATP (*SI Appendix*, Fig. S4*C*). Both regions, (247 to 270, 273 to 299) were located on the ankyrin repeats and showed more than 10% decreases in deuteration level. None of the catalytic domain or linker peptide regions showed significant deuteration level changes.

The time course of the hydrogen/deuterium exchange in these peptide regions is shown in Fig. 2*A*. The peptide region 247 to 270 showed an average of 2.1 deuterons (10%) decrease of exchange in the whole-time course and showed the maximum 3.7 deuterons (17%) decrease of exchange at 3,000 s. Since region 253 to 274 did not show changes upon ATP binding, we hypothesize that region 247 to 252 might be responsible for the decrease of deuteration, accounting for an average 42% decrease and a maximal 74% decrease at 3,000 s. We also observed significant changes in other regions, 273 to 299 (average 2.7 deuterons, 11%), 277 to 299 (average 2.2 deuterons, 11%), and 286 to 299 (average 1.4 deuterons, 11%) showing similar levels of decrease in exchange. Region 273 to 299 contains multiple positively charged residues, including Lys282, Arg285, and Lys295 (Fig. 2*B*), which may contribute to the binding of the ATP triphosphate groups.

To confirm the hypothesis that the $iPLA_2$ inhibition by calcium di-cations is through preventing ATP binding, the calcium inhibition effects were further monitored using hydrogen/deuterium exchange. Since the peptide regions 247 to 270 and 277 to 299 showed decreased deuteration upon ATP binding, increase of deuteration levels of these peptide regions would confirm the

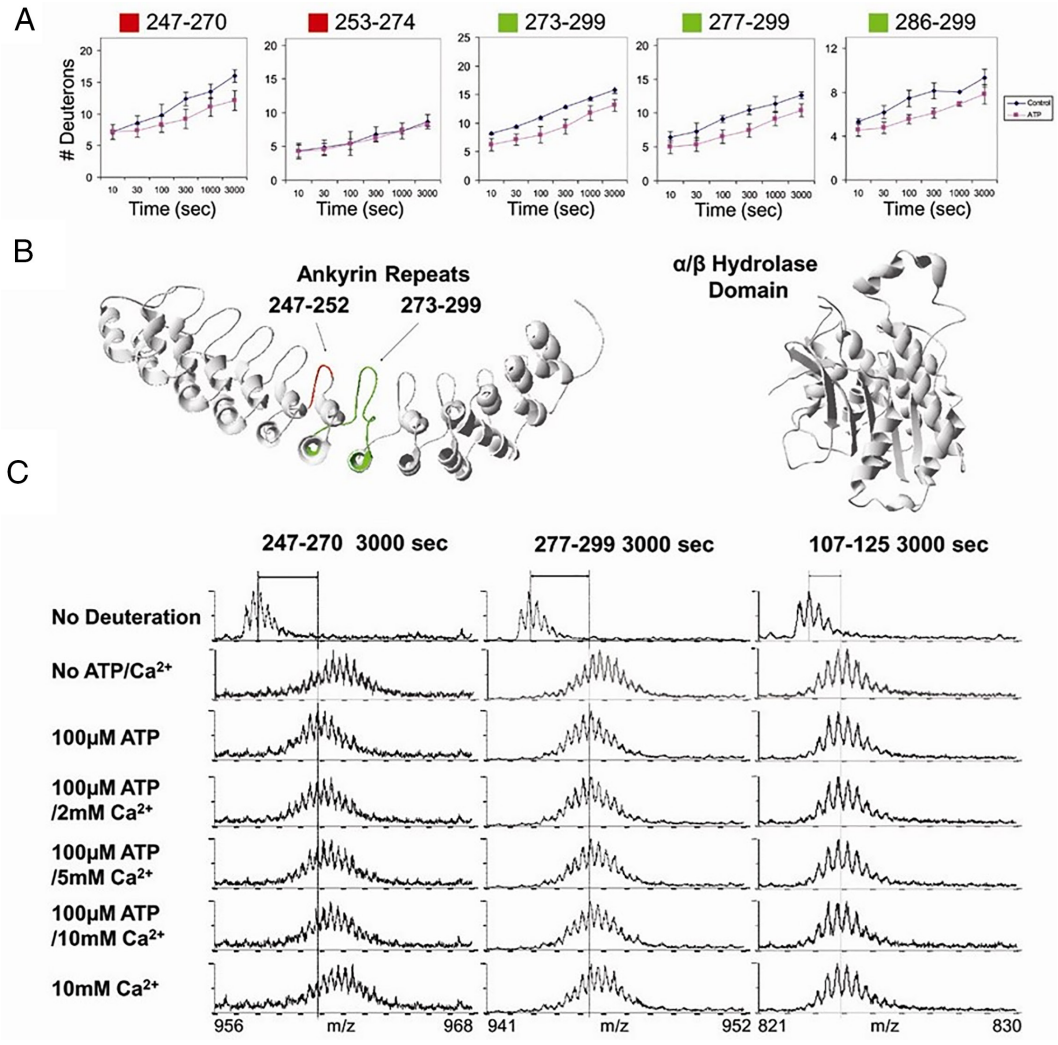

Fig. 2. HDX-MS for identifying the peptide regions interacting with ATP and for studying the inhibition effects of calcium. (*A*) Hydrogen/Deuterium exchange time courses of the regions affected by ATP binding. The number of incorporated deuterons in $iPLA_2$ without (◆) and with 1 mM of ATP (■) are shown for peptide regions that deuteration levels were changed upon ATP binding. Averages of three individual experiments are shown. The scale of the *Y*-axis is the maximum deuteron number, (*B*) The ATP binding regions identified by HDX-MS are localized on the ankyrin repeats. The presented homology model is based on the crystal structures of human Ankyrin-R (PDB ID: 1N11) and patatin (PDB ID: 1OXW) and (*C*) Calcium increases deuteration level of the peptide regions found to interact with ATP. The mass envelopes in the regions 247 to 270 and 277 to 299 are shown at various calcium concentrations. The region 107 to 125 was used as a control and it does not show any changes.

interference of calcium di-cations with ATP binding. $iPLA_2$ was deuterated at various concentrations of calcium for 3,000 s and the deuteration results for peptide regions 247 to 270 and 277 to 299 are shown in Fig. 2*C*. The mass envelopes of the nondeuterated isotopic peaks are shown in the first panel. The dashed line indicates the mass/charge average of the nondeuterated peptide fragment. The shift of the peak relative to the nondeuterated sample peak is the deuterium retained in the fragment. After 3,000 s of hydrogen/deuterium exchange, the deuteration caused the peaks in all conditions to shift to a higher mass/charge. The second panel shows the deuterated mass envelopes of $iPLA_2$ without calcium or ATP. The ATP-bound form of $iPLA_2$ in the third panel shows a significant mass decrease in regions 247 to 270 and 277 to 299 and is the reference point for monitoring the calcium inhibition effect. Peptide regions 247 to 270 and 277 to 299 at various concentrations of calcium caused the peak shift to higher mass. The effects of deuteration increase are larger at a higher concentration of calcium and at concentration of 10 mM of calcium the peak showed the greatest shift. At 2 mM calcium concentration, the peak showed about half of the total shift, which coordinated with the apparent Km of 1.6 mM. This also indicates that the HDX-MS peak shift coordinates well with the kinetic results. These results confirmed the hypothesis that the calcium inhibition of $iPLA_2$ activity is achieved through the interference of the calcium with ATP.

Defining Calmodulin Binding Effects on $iPLA_2$ Using HDX-MS. Calmodulin is a negative allosteric regulator of $iPLA_2$, and it has been reported to inhibit $iPLA_2$ activity through direct physical interaction that causes a conformational change near the active site of the enzyme (27). Understanding the calmodulin inhibition mechanism and the mechanism of reactivation of calmodulin inhibited $iPLA_2$ could potentially open the road to the development of novel therapeutics by modulating the activity in various pathological conditions in which $iPLA_2$ is involved. Hydrogen/deuterium exchange experiments on calmodulin binding were performed in the absence of ATP with 500 μM of calcium. To ensure the proper binding between calmodulin and $iPLA_2$, the final concentration of 18 μM calmodulin (50 μg) was 7.5 times the 2.4 μM $iPLA_2$. Since excess amounts of calmodulin cannot bind to $iPLA_2$, only the hydrogen/deuterium exchange of $iPLA_2$ was monitored. Some calmodulin-generated peaks overlapped with the mass envelopes from the $iPLA_2$ peptides. Because of the presence of the extra peaks from calmodulin, some $iPLA_2$ peaks showed dramatic apparent increases of deuteration. These peptides were manually examined, and the overlapped peptides were removed for the analysis.

The only region that showed changes upon calmodulin binding was at the N-terminal region 20 to 28. This region showed an average 0.7 deuteron (9%) and a maximum 1.1 deuteron (14%) decrease of deuteration when the calmodulin bound to the N-terminal region. The sequence of this peptide is shown in *SI Appendix*, Fig. S5, and it has a region of alternating positively charged residues and hydrophobic residues. Positively charged amphipathic helices were reported to play an important role in the binding of calmodulin which is consistent with the HDX-MS data (36). To confirm that effect was not caused by nonspecific binding, we added EDTA in addition to Calcium/Calmodulin in the hydrogen/deuterium exchange experiments. EDTA eliminated the changes caused by calmodulin, indicating that the effects on region 20 to 28 were from the association with activated calmodulin. We also detected three individual fragments in the previously hypothesized calmodulin binding region (residues 745 to 770). The region 760 to 767 containing the partial binding region did not show significant changes in hydrogen/deuterium exchange. Two other peptides (residues 753 to 757 and 756 to 769) in this binding region overlapped with a peak from calmodulin making it impossible to track the on-exchange rates for these peptides. Based on the monoisotopic and the M+1 peak, which were not affected by the calmodulin peak, no significant changes were observed for these peptides. These results suggested that the N-terminal region is mostly responsible for calmodulin binding. It is worth noting that previously published studies suggested that calmodulin binds to two putative peptides containing the canonical IQ and 1-9-14 motifs (aa 622 to 635) in the hamster GVIA-1 $iPLA_2$ structure (whose sequence is similar to the originally isolated P388D1 macrophage GVIA-1) (16, 22, 37, 38). However, in our studies on the human GVIA-2 $iPLA_2$ enzyme, these peptides did not exhibit any decreased deuteration.

Discussion

Since the discovery of $iPLA_2$, it has been known that ATP and other di- and triphosphate nucleosides enhance the enzymatic activity of this enzyme suggesting that they are activators (22). However, it has not been clear whether ATP is a kinetic activator or a binding partner that stabilizes and maintains the activity of $iPLA_2$ (29). In an in vitro assay, where no other regulating protein could interfere, ATP was found to be an activator of $iPLA_2$ with a very low apparent Km of 0.9 μM (*SI Appendix*, Fig. S1*A*). In healthy cells, ATP is about 1 to 10 mM which is 1,000-fold higher than the apparent Km, and thus is sufficient to activate $iPLA_2$. Other studies showed that ATP protected $iPLA_2$ from cysteine oxidation to maintain its activity over time (30). In a complex cellular environment it is possible that oxidation of $iPLA_2$ could occur under oxidative stress, and thus, in such conditions, it is possible that ATP prevents $iPLA_2$ oxidation. Regarding the GVIA-1 and GVIA-2 $iPLA_2$, it was reported that GVIA-1 is not activated by ATP although GVIA-1 interacts with ATP (16, 39). The 54 amino acid insertion in the GVIA-2 $iPLA_2$ (aa 396 to 449) disrupts the ninth ankyrin repeat and makes it a linker but does not affect the ATP binding region.

ATP Binding Site on ARD. To elucidate the binding mode of ATP on the $iPLA_2$ ankyrin repeats, MD simulations were performed using a previously described homology model of the $iPLA_2$ ankyrin repeats (24). The MD simulations were conducted on the ankyrin repeats of $iPLA_2$ connected to the catalytic domain using a system that contained five randomly placed ATP molecules located approximately 10 Å away from the protein. The system was solvated with explicit water molecules and subjected to a two microsecond MD simulation (Movie S1). The MD simulation showed an ATP molecule diffusing from the solvent and starting to interact with $iPLA_2$ at a site consisting of the peptide regions 247 to 270 and 273 to 299. After approximately 300 ns the ATP molecule was fully bound to the site and its conformation was stable during the rest of the simulation indicating that the molecule adopted a stable conformation (Fig. 3*A*). The main interactions include hydrogen bonding of the triphosphate moiety with Lys261 and Lys295 which are part of the peptide regions that showed decreased deuteration levels and with additional residues like Arg327 and Arg329. These four residues constitute a positively charged cluster that stabilizes the triphosphate moiety. The aromatic ring of adenine is placed in a highly aromatic pocket consisting of residues Pro251, Asn252, Tyr254, His257, Tyr286, Trp293, Ala288, Pro290, and His292. These residues are located in the peptide regions that showed decreased deuteration levels and participate in pi stacking and aromatic–aliphatic interactions

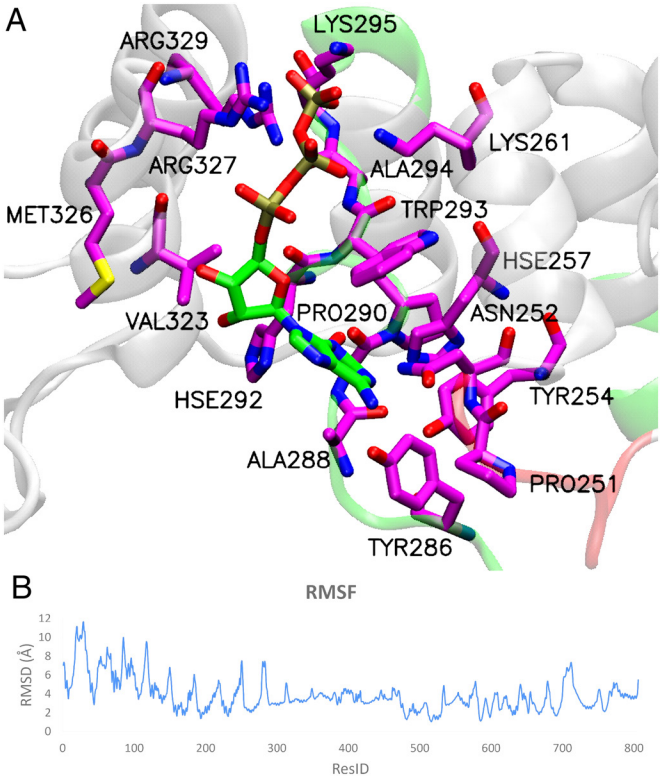

Fig. 3. MD simulations of $iPLA_2$ in the presence of ATP molecules (Movie S1). (*A*) The binding mode and interactions of ATP after two microseconds simulation (HSE = HIS = Histidine), and (*B*) RMS fluctuation (RMSF) of $iPLA_2$ residues during the simulation.

with the aromatic ring of adenine. Two additional hydrogen bonds between the triphosphate group and Trp293, and between the amine of the adenine ring with Tyr254 were observed. It is worth mentioning that previously published structural studies on the hamster enzyme suggested that ATP binds at a site near Trp293 that is now fully characterized by our studies (16). Based on Rms fluctuation analysis, stabilization of this region was observed upon ATP binding (Fig. 3*B*). Residues 247 to 253 showed RMSF values between 5 to 7.5Å which is consistent with the lack of interactions with ATP, while residues 254 to 270 showed RMSF values between 2.1 to 2.7 Å indicating stabilization due to interactions. Similarly, residues 273 to 287 showed RMSF values between 3 to 7.5 Å while residues 288 to 299 showed RMSF values between 2.8 to 3.0 Å due to interactions with ATP.

The crystal structure of the ankyrin repeats of the transient receptor potential cation channel TRPV1 showed that ATP can bind to ankyrin repeats and regulate the calcium channels in a completely different ATP binding mechanism compared to protein kinases, which does not require metal ions (40). Similarly to TRPV1, the ATP could bind to the ankyrin repeats of $iPLA_2$ and cause a conformational change that enhances the activity of the enzyme, even though the residues of $iPLA_2$ ATP binding site differ. According to the HDX-MS and MD simulations, the ATP binds to region 247 to 299 in $iPLA_2$ near to the 5th and 6th ankyrin repeats. The ATP binding site in TRPV1 matches the unstable region of the ARD. It is worth mentioning that these repeating elements are stably packed side by side but the folding on both ends of the 5th and 6th ankyrin repeats indicates higher strain energy, and thus these regions are more flexible (41–43). It is worth noting that the ATP binding site in TRPV1 also shows regions of high strain energy in the ARD. Binding of the ATP molecule in these regions might result in lower energy through conformational changes triggered by ATP interactions. This might be a potential mechanism of allosteric regulation of $iPLA_2$ by ATP. Presumably these conformational changes cause a subtle change in the $iPLA_2$ active site conformation which results in an improved conformation for catalysis in the active site and catalytic activation.

Verifying the ATP Binding Site Using Mutagenesis. To further validate the identified using HDX-MS and MD simulations binding site of ATP on the $iPLA_2$ ARD, several mutants were generated to examine the effect of ATP on the $iPLA_2$ activity. The following residues including K261, Y286, W293, and R329 were mutated to alanine and tested for their activity in the presence and absence of ATP using a lipidomics-based assay and PLPC or PAPC as substrates. Residues like K261, Y286, and W293 were part of the peptide regions that showed decrease on deuteration levels, while R329 is one of the additional charged residues identified with MD simulations. All mutants showed a significantly low response to ATP in both substrates, although K261A still showed activation by ATP (Fig. 1 *C* and *D*). Notably, Y286A, W293A, and R329A mutants completely lost the response to ATP. These results showed that these residues suggested by HDX-MS and the MD simulation affect the ATP activation of $iPLA_2$ in support of the binding model. It is worth mentioning that the basal $iPLA_2$ activity in the absence of ATP was somehow affected by these mutations. However, the difference was insignificant and not greater than the effect of ATP. None of the mutants lost their basal activity indicating that the mutations did not affect the structure of the $iPLA_2$. The basal activity of K261A and R329A toward PLPC without ATP was slightly higher than the WT, while the activity of Y286A and W293A was slightly lower than that of WT (*SI Appendix*, Fig. S6*B*). The activation effect of ATP on $iPLA_2$ was found to be different for PLPC and PAPC (12-fold and 4.5-fold activation, respectively) (Fig. 1 *C* and *D*), which is consistent with previous studies showing that $iPLA_2$ prefers PLPC over PAPC by more than twofold (6).

To further confirm the direct binding between the putative ATP binding site and ATP, a precipitation assay using ATP-conjugated agarose and purified ARD-His was performed. The binding was assessed by eluting bound ARD-His from the ATP agarose with 10 mM ATP and detecting the amount of ARD-His in the elution by western blot. Although some amount of ARD was nonspecifically eluted by the buffer without ATP, a higher fraction of ARD was eluted by 10 mM ATP (Fig. 4*A*). Confirming the dependence of the amount of eluted ARD-His on the concentration of ATP demonstrated the direct binding of ARD to the ATP (Fig. 4*B*). The same experiment was performed on Y286A, W293A, and R329A mutants of ARD-His. While Y286A mutant showed reduced binding of ARD to the ATP agarose with no statistical significance compared to that of WT, W293A, and R329A mutants significantly attenuated the binding to ATP up to 80% (Fig. 4*C*). These results indicated that ATP directly binds to GVIA $iPLA_2$ ARD through the residues identified by the HDX-MS and MD simulation to allosterically enhance the enzymatic activity. These results revealed that W293 and R329 are essential residues ATP binding and that Y286 even though does not show statistically significant reduction, it might be important for the ATP response (Figs. 1 *C* and *D* and 4*C*).

It is worth mentioning that $iPLA_2$ mutations that were reported to suppress the enzymatic activity are involved in neurodegeneration diseases such as dystonia-parkinsonism, infantile neuroaxonal dystonia (INAD), brain iron accumulation (NBIA) disorders, and atypical neuroaxonal dystrophy (44). Among them, R329 that found in this study as the critical residue for ATP binding, is

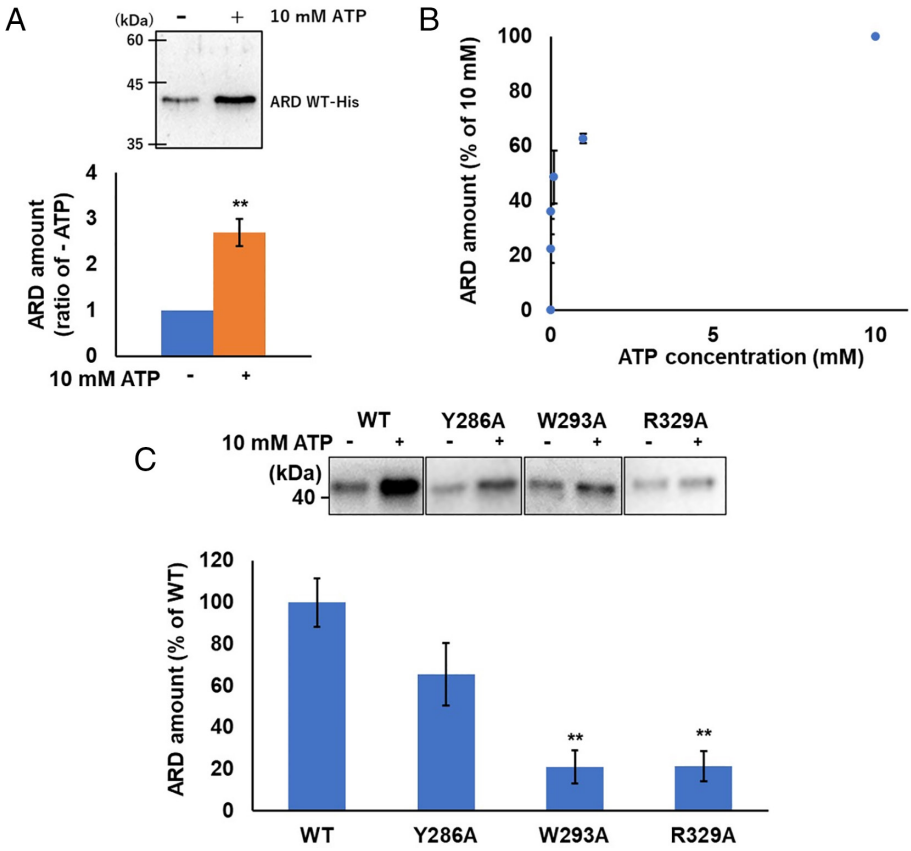

Fig. 4. Direct binding between ATP and ARD. (*A*) The western blot analysis of eluted purified-ARD-His from ATP agarose by 10 mM ATP, (*B*) Concentration-dependent effect of ATP on the elution of ARD-His from the ATP agarose, and (*C*) The effect of the putative ATP binding site mutants on the binding to the ATP agarose. The amount of purified ARD WT and mutants subjected to the binding assay was normalized by its expression in such that the same quantity of ARDs were incubated with ATP beads. The amount of ARD-His was detected by His tag antibody. The intensity of each band was measured by Image J. The values are presented as the mean ± SD. Asterisks indicate statistical significance (**$P < 0.01$).

a highly conserved amino acid across different species, and mutation of this amino acid are known to cause INAD (45). These facts indicate the importance of ATP binding in the physiological role of $iPLA_2$ and open the road to the development of novel therapeutics that target the activation of mutated $iPLA_2$ through the ATP binding site.

Conclusion

The regulatory role of ATP in enhancing the activity of $iPLA_2$ involves a sophisticated interplay with its ARD. Initial investigations pinpointed two crucial peptide regions, spanning amino acids 247 to 270 and 273 to 299, as pivotal in understanding how ATP interacts with these repeats. Employing MD simulations provided invaluable insights into the precise binding mechanism of ATP to the ankyrin repeats. The simulations unveiled a detailed binding motif where ATP establishes robust interactions with specific residues. Notably, the triphosphate moiety of ATP forms hydrogen bonds with a cluster of charged residues, including Lys261, Lys295, Arg327, and Arg329. The adenine ring of ATP snugly fits into an aromatic pocket constituted by residues Pro251, Asn252, Tyr254, His257, Tyr286, Trp293, Ala288, Pro290, and His292.

To validate these findings, site-directed mutagenesis experiments and a precipitation assay utilizing ATP-conjugated agarose were conducted. These experiments unequivocally confirmed the presence of an ATP binding site within the ARD of $iPLA_2$. Overall, these findings underscore the significance of ATP binding in modulating the physiological function of $iPLA_2$. Furthermore, they pave the way for the development of innovative therapeutic approaches targeting the activation of mutated forms of $iPLA_2$ through manipulation of the ATP binding site. Such interventions hold promise for addressing various pathological conditions associated with dysregulated $iPLA_2$ activity.

Data, Materials, and Software Availability. All study data are included in the article and/or supporting information.

ACKNOWLEDGMENTS. Work on this manuscript was supported by National Institute of General Medical Sciences Maximizing Investigators' Research Award grant R35 GM139641, which is a renewal of RO1 GM20501-44, which supported all of the early work on $iPLA_2$ in our laboratory (E.A.D.)

Author affiliations: [a]Department of Chemistry and Biochemistry, University of California San Diego, La Jolla, CA 92093-0601; [b]Department of Pharmacology, School of Medicine, University of California San Diego, La Jolla, CA 92093-0601; [c]Department of Applied Chemistry in Bioscience, Graduate School of Agricultural Science, Kobe University, Kobe 657-8501, Japan; and [d]Department of Medicine, School of Medicine, University of California, San Diego, La Jolla, CA 92093

1. E. Dennis, J. Cao, Y.-H. Hsu, V. Magrioti, G. Kokotos, Phospholipase A2 enzymes: Physical structure, biological function, disease implication, chemical inhibition, and therapeutic intervention. *Chem. Rev.* **111**, 6130–6185 (2011).
2. V. D. Mouchlis, E. A. Dennis, Membrane association allosterically regulates phospholipase A2 enzymes and their specificity. *Acc. Chem. Res.* **55**, 3303–3311 (2022).
3. V. D. Mouchlis, T. M. Mavromoustakos, G. Kokotos, Molecular docking and 3D-QSAR CoMFA studies on indole inhibitors of GIIA secreted phospholipase A2. *J. Chem. Inf. Model.* **50**, 1589–1601 (2010).
4. V. D. Mouchlis, D. Bucher, J. A. McCammon, E. A. Dennis, Membranes serve as allosteric activators of phospholipase A2, enabling it to extract, bind, and hydrolyze phospholipid substrates. *Proc. Natl. Acad. Sci. U.S.A.* **112**, E516–E525 (2015).

5. A. M. Vasquez, V. D. Mouchlis, E. A. Dennis, Review of four major distinct types of human phospholipase A2. *Adv. Biol. Regul.* **67**, 212–218 (2018).
6. V. D. Mouchlis, Y. Chen, J. A. McCammon, E. A. Dennis, Membrane allostery and unique hydrophobic sites promote enzyme substrate specificity. *J. Am. Chem. Soc.* **140**, 3285–3291 (2018).
7. V. D. Mouchlis, E. A. Dennis, Phospholipase A2 catalysis and lipid mediator lipidomics. *Biochim. Biophys. Acta Mol. Cell Biol. Lipids* **1864**, 766–771 (2019).
8. D. Hayashi, E. A. Dennis, Molecular basis of unique specificity and regulation of group VIA calcium-independent phospholipase A2 (PNPLA9) and its role in neurodegenerative diseases. *Pharmacol. Ther.* **245**, 108395 (2023).
9. M. Basselin *et al.*, Imaging decreased brain docosahexaenoic acid metabolism and signaling in iPLA2β (VIA)-deficient mice. *J. Lipid Res.* **51**, 3166–3173 (2010).
10. L. A. Engel, Z. Jing, D. E. O'Brien, M. Sun, P. T. C. Kotzbauer, Catalytic function of PLA2G6 is impaired by mutations associated with infantile neuroaxonal dystrophy but not dystonia-parkinsonism. *PLoS One* **5**, e12897 (2009).
11. A. Malhotra *et al.*, Role of calcium-independent phospholipase A2 in the pathogenesis of Barth syndrome. *Proc. Natl. Acad. Sci. U.S.A.* **106**, 2337–2341 (2009).
12. A. Gregory *et al.*, Neurodegeneration associated with genetic defects in phospholipase A(2). *Neurology* **71**, 1402–1409 (2008).
13. S. Ayilavarapu *et al.*, Diabetes-induced oxidative stress is mediated by Ca^{2+}-independent phospholipase A2 in neutrophils. *J. Immunol.* **184**, 1507–1515 (2010).
14. R. N. Bone *et al.*, Inhibition of Ca^{2+}-independent phospholipase A2β (iPLA2β) ameliorates islet infiltration and incidence of diabetes in NOD mice. *Diabetes* **64**, 541–555 (2015).
15. C. Cavestro *et al.*, Novel deep intronic mutation in PLA2G6 causing early-onset Parkinson's disease with brain iron accumulation through pseudo-exon activation. *Neurogenetics* **22**, 347–351 (2021).
16. K. R. Malley *et al.*, The structure of iPLA2β reveals dimeric active sites and suggests mechanisms of regulation and localization. *Nat. Commun.* **9**, 765 (2018).
17. A. Kalyvas *et al.*, Differing roles for members of the phospholipase A2 superfamily in experimental autoimmune encephalomyelitis. *Brain* **132**, 1221–1235 (2009).
18. Y.-H. Hsu *et al.*, Fluoroketone inhibition of Ca^{2+}-independent phospholipase A2 through pinding pocket association defined by hydrogen/deuterium exchange and molecular dynamics. *J. Am. Chem. Soc.* **135**, 1330–1337 (2013).
19. V. D. Mouchlis *et al.*, Development of potent and selective inhibitors for group VIA calcium-independent phospholipase A2 guided by molecular dynamics and structure-activity relationships. *J. Med. Chem.* **59**, 4403–4414 (2016).
20. V. D. Mouchlis, A. Armando, E. A. Dennis, Substrate-specific inhibition constants for phospholipase A2 acting on unique phospholipid substrates in mixed micelles and membranes using lipidomics. *J. Med. Chem.* **62**, 1999–2007 (2019).
21. V. D. Mouchlis, C. Mu, R. Hammons, E. A. Dennis, Lipidomics-based assays coupled with computational approaches can identify novel phospholipase A2 inhibitors. *Adv. Biol. Regul.* **76**, 100719 (2020).
22. E. J. Ackermann, E. S. Kempner, E. A. Dennis, Ca^{2+}-independent cytosolic phospholipase A2 from macrophage-like P388D1 cells. Isolation and characterization. *J. Biol. Chem.* **269**, 9227–9233 (1994).
23. P. K. Larsson, H. E. Claesson, B. P. Kennedy, Multiple splice variants of the human calcium-independent phospholipase A2 and their effect on enzyme activity. *J. Biol. Chem.* **273**, 207–214 (1998).
24. Y.-H. Hsu, J. Burke, S. Li, V. Woods, E. Dennis, Localizing the membrane binding region of Group VIA Ca^{2+}-independent phospholipase A2 using peptide amide hydrogen/deuterium exchange mass spectrometry *J. Biol. Chem.* **284**, 23652–23661 (2009).
25. D. Bucher, Y. H. Hsu, V. D. Mouchlis, E. A. Dennis, J. A. McCammon, Insertion of the Ca^{2+}-independent phospholipase A2 into a phospholipid bilayer via coarse-grained and atomistic molecular dynamics simulations *PLoS Comput. Biol.* **9**, e1003156 (2013).
26. J. Y. Liou *et al.*, Mitochondrial localization of cyclooxygenase-2 and calcium-independent phospholipase A2 in human cancer cells: Implication in apoptosis resistance. *Exp. Cell Res.* **306**, 75–84 (2005).
27. C. M. Jenkins, M. J. Wolf, D. J. Mancuso, R. W. Gross, Identification of the calmodulin-binding domain of recombinant calcium-independent phospholipase A2beta. Implications for structure and function. *J. Biol. Chem.* **276**, 7129–7135 (2001).
28. Z. Ma, S. Zhang, J. Turk, S. Ramanadham, Stimulation of insulin secretion and associated nuclear accumulation of iPLA2β in INS-1 insulinoma cells. *Am. J. Physiol. Endocrinol. Metab.* **282**, E820–E833 (2002).
29. Y. C. Lio, E. A. Dennis, Interfacial activation, lysophospholipase and transacylase activity of group VI Ca^{2+}-independent phospholipase A2. *Biochim. Biophys. Acta* **1392**, 320–332 (1998).
30. H. Song, S. Bao, S. Ramanadham, J. Turk, Effects of biological oxidants on the catalytic activity and structure of group VIA phospholipase A2. *Biochemistry* **45**, 6392–6406 (2006).
31. J. Zheng *et al.*, 2.2 A refined crystal structure of the catalytic subunit of cAMP-dependent protein kinase complexed with MnATP and a peptide inhibitor. *Acta Crystallogr. D Biol. Crystallogr.* **49**, 362–365 (1993).
32. D. Chin, A. R. Means, Calmodulin: A prototypical calcium sensor. *Trends Cell Biol.* **10**, 322–328 (2000).
33. P. Michaely, D. Tomchick, M. Machius, R. Anderson, Crystal structure of a 12 ANK repeat stack from human ankyrinR. *EMBO J.* **21**, 6387–6483 (2002).
34. Y.-H.H. Hsu *et al.*, Calcium binding rigidifies the C2 domain and the intradomain interaction of GIVA phospholipase A2 as revealed by hydrogen/deuterium exchange mass spectrometry. *J. Biol. Chem.* **283**, 9820–9827 (2008).
35. T. J. Rydel *et al.*, The crystal structure, mutagenesis, and activity studies reveal that patatin is a lipid acyl hydrolase with a Ser-Asp catalytic dyad. *Biochemistry* **42**, 6696–6708 (2003).
36. W. G. Thomas, L. Pipolo, H. Qian, Identification of a Ca^{2+}/calmodulin-binding domain within the carboxyl-terminus of the angiotensin II (AT1A) receptor. *FEBS Lett.* **455**, 367–371 (1999).
37. M. A. Balboa, J. Balsinde, S. S. Jones, E. A. Dennis, Identity between the Ca^{2+}-independent phospholipase A2 enzymes from P388D1 macrophages and Chinese hamster ovary cells *J. Biol. Chem.* **272**, 8576–8580 (1997).
38. J. Tang *et al.*, A novel cytosolic calcium-independent phospholipase A2 contains eight ankyrin motifs. *J. Biol. Chem.* **272**, 8567–8575 (1997).
39. Z. Ma, X. Wang, W. Nowatzke, S. Ramanadham, J. C. Turk, Human pancreatic islets express mRNA species encoding two distinct catalytically active isoforms of group VI phospholipase A2 (iPLA2) that arise from an exon-skipping mechanism of alternative splicing of the transcript from the iPLA2 gene on chromosome 22q13.1. *J. Biol. Chem.* **274**, 9607–9616 (1999).
40. P. V. Lishko, E. Procko, X. Jin, C. B. Phelps, R. Gaudet, The ankyrin repeats of TRPV1 bind multiple ligands and modulate channel sensitivity. *Neuron* **54**, 905–918 (2007).
41. D. U. Ferreiro, J. A. Hegler, E. A. Komives, P. G. Wolynes, Localizing frustration in native proteins and protein assemblies. *Proc. Natl. Acad. Sci. U.S.A.* **104**, 19819–19824 (2007).
42. D. U. Ferreiro, A. M. Walczak, E. A. Komives, P. G. Wolynes, The energy landscapes of repeat-containing proteins: Topology, cooperativity, and the folding funnels of one-dimensional architectures. *PLoS Comput. Biol.* **4**, e1000070 (2008).
43. D. U. Ferreiro, P. G. Wolynes, The capillarity picture and the kinetics of one-dimensional protein folding. *Proc. Natl. Acad. Sci. U.S.A.* **105**, 9853–9854 (2008).
44. M. A. Illingworth *et al.*, PLA2G6-associated neurodegeneration (PLAN): Further expansion of the clinical, radiological and mutation spectrum associated with infantile and atypical childhood-onset disease. *Mol. Genet. Metab.* **112**, 183–189 (2014).
45. S. Kapoor *et al.*, Genetic analysis of PLA2G6 in 22 Indian families with infantile neuroaxonal dystrophy, atypical late-onset neuroaxonal dystrophy and dystonia parkinsonism complex. *PLoS One* **11**, e0155605 (2016).